

# Multimode Vibrational Strong Coupling of Methyl Salicylate to a Fabry–Pérot Microcavity

Wassie Mersha Takele, Frank Wackenhut,<sup>\*,†</sup> Lukasz Piatkowski,<sup>\*,†</sup> Alfred J. Meixner, and Jacek Waluk

Cite This: *J. Phys. Chem. B* 2020, 124, 5709–5716

Read Online

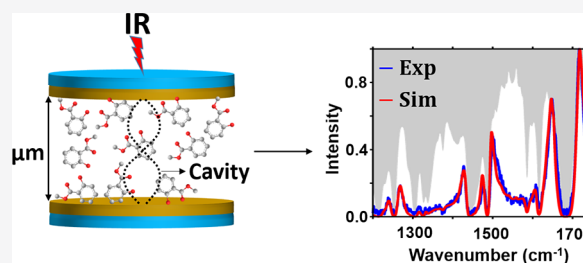
ACCESS |

Metrics & More

Article Recommendations

Supporting Information

**ABSTRACT:** The strong coupling of an IR-active molecular transition with an optical mode of the cavity results in vibrational polaritons, which opens a new way to control chemical reactivity via confined electromagnetic fields of the cavity. In this study, we design a voltage-tunable open microcavity and we show the formation of multiple vibrational polaritons in methyl salicylate. A Rabi splitting and polariton anticrossing behavior is observed when the cavity mode hybridizes with the C=O stretching vibration of methyl salicylate. Furthermore, the proposed theoretical model based on coupled harmonic oscillators reveals that the absorption of uncoupled molecules must also be considered to model the experimental spectra properly and that simultaneous coupling of multiple molecular vibrations to the same cavity mode has a significant influence on the transmission spectral profile.



## INTRODUCTION

When molecules are placed within an optical microcavity, their quantized transitions can exchange energy with the cavity mode once the resonant condition is met.<sup>1,2</sup> If the rate of energy exchange is faster than the decay rates of both constituents, the system enters the so-called strong coupling (SC) regime.<sup>3</sup> SC leads to the formation of hybrid light–matter states called polaritons.<sup>4,5</sup> Since this opens a way to tune energy levels,<sup>6,7</sup> SC has emerged as an intriguing platform to actively control molecular and material properties.<sup>8–15</sup> For instance, strong coupling of electronic excited states with the cavity mode has been used to modulate energy transfer,<sup>16</sup> conductivity,<sup>17</sup> Stokes shift,<sup>18</sup> quantum yield of emission,<sup>19</sup> and work function.<sup>20</sup> Recently, these ideas have been extended to a novel field of vibrational strong coupling (VSC), where chemical reactivity can be altered by the zero-point-energy fluctuations of the optical mode of a cavity.<sup>21–23</sup>

VSC is attained when IR-active molecular vibrations hybridize with the vacuum electric field of an IR microcavity.<sup>24</sup> As a consequence, a vibrational transition splits into lower (VP<sup>-</sup>) and higher (VP<sup>+</sup>) vibrational polaritons,<sup>25,26</sup> separated by the Rabi splitting energy ( $\hbar\Omega_R$ ), which is illustrated in Figure 1a. The splitting depends on the molecular transition dipole moment ( $\mu$ ), the cavity electric field ( $E_{\text{cav}}$ ) and the concentration ( $C$ ),  $\hbar\Omega_R \propto \mu \cdot E_{\text{cav}} \cdot \sqrt{C}$ .<sup>6,26</sup> Vibrational polaritons have been observed from pure organic liquids,<sup>26</sup> polymer films,<sup>27–29</sup> organometallic complexes dissolved in water,<sup>30</sup> a liquid crystal molecule,<sup>25</sup> and different molecules simultaneously dissolved in solution.<sup>31</sup> So far, VSC has been employed to suppress<sup>32</sup> or enhance<sup>33</sup> the rate of chemical reactions and even to alter reaction selectivity.<sup>34</sup> Recently, Vergauwe et al. showed the modification of the rate of an enzymatic hydrolysis

reaction under strong coupling involving the water vibrations.<sup>35</sup> An intriguing idea is to alter/control intramolecular reactions to tailor the photophysics and/or excited state reactivity of a molecule. Fascinating examples are molecules exhibiting excited state intramolecular proton transfer, for instance, methyl salicylate (MS)—see Figure 1b for the molecular structure—which we selected as a model system for our studies. It has been demonstrated for several proton/hydrogen-transferring systems that different vibrational modes contribute simultaneously to the tautomerization reaction coordinate.<sup>36–38</sup> One can therefore envision that knowing, based on the type of experiments shown here together with the appropriate modeling, which molecular modes couple to the cavity modes and with what strengths, it would be possible to find a cavity setting that would influence the reaction coordinate more effectively than in the case of simple one-to-one (single mode-to-mode) coupling. We believe that coupling to multiple vibrational reaction coordinates may be more effective in modulating the reaction than in the case of single reaction coordinate coupling. Obviously, it is the excited state vibration that affects the photoinduced processes. In principle, our setup should allow looking for excited state effects by monitoring changes caused by detuning the cavity from the ground state coupling toward the excited state

Received: April 29, 2020

Revised: June 13, 2020

Published: June 15, 2020



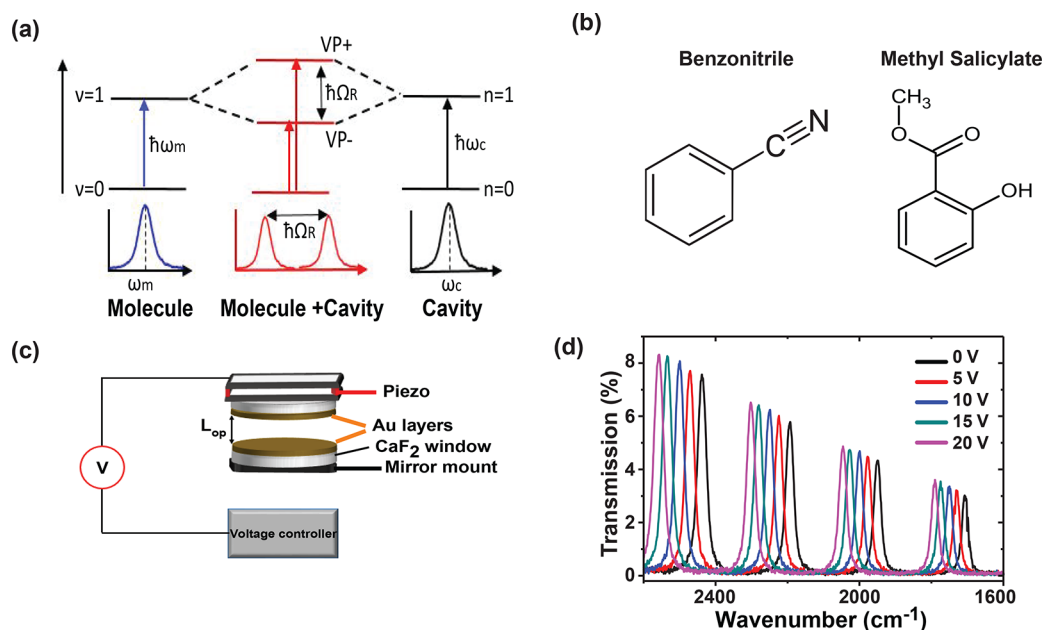


**Figure 1.** (a) Schematic illustration of the strong coupling effect between a vibrational transition ( $\nu = 0 \rightarrow \nu = 1$ ) and an optical microcavity mode ( $n = 0 \rightarrow n = 1$ ). When the vibrational frequency of a molecular transition ( $\omega_m$ ) matches the resonant frequency of a cavity mode ( $\omega_c$ ), the two states hybridize and split into two new states: lower ( $VP^-$ ) and upper ( $VP^+$ ) vibrational polaritons, separated by the Rabi splitting ( $\hbar\Omega_R$ ). (b) Molecular structure of benzonitrile and methyl salicylate. (c) Schematic illustration of the Fabry–Pérot type open microcavity structure used to couple liquid phase samples. (d) Transmission spectrum of an empty microcavity, as a function of voltage applied to a piezoelectric element of the mirror holder.

frequency. Thus, as a prelude to controlling photoinduced tautomerization through VSC, we investigate here the properties of MS in the strong coupling regime.

In most of the previous studies,<sup>26–31</sup> VSC was typically realized using a fixed thickness microcavity, for which the resonant frequency is tuned by tilting the sample with respect to the light propagation direction. However, in this work, we made use of a voltage-tunable open Fabry–Pérot microcavity that can be brought into resonance with any vibrational transition without moving and/or rotating the sample; thereby it could be an important tool for the growing field of VSC. Coupling of two vibrational frequencies from a single molecular species with a cavity mode was first reported by George et al.,<sup>26</sup> while Menghrajani et al.<sup>39</sup> recently demonstrated the hybridization of three vibrational resonances of a polymer film with the same cavity mode. Two other papers<sup>29,40</sup> discussed hybridized polaritons generated by simultaneous strong coupling of the cavity mode with two or more vibrational transitions in different organic materials. Yet the work of Erwin et al.<sup>41</sup> focused on the role of bulk vibrations. They showed that the bulk molecular vibrations are changed by interaction within the cavity, even though they are not in dressed states. Here, we attempt to assess the contributions from both, dressed and “dark” states by comparing the experimental spectra with the simulations carried out at various levels of theory. We show that multiple vibrations from MS solution, even those seemingly off resonant, can be simultaneously hybridized to the same cavity mode. To examine the influence of this complex multimode coupling behavior on the Rabi splitting, we develop a theoretical model based on a damped harmonic oscillator. We demonstrate that, for the proper simulation of the experiment, the absorption of uncoupled molecular oscillators has to be taken into account.

## METHODS

Methyl salicylate (99%), methylcyclohexane (99%), and benzonitrile (BN, 99%) were purchased from Sigma-Aldrich and used without further purification. CaF<sub>2</sub> windows ( $d = 25.0$  mm, 5.0 mm thickness) were purchased from Crystran Ltd., while mirror mounts with piezoelectric control were purchased from Thorlabs, Inc.

**Open Microcavity Preparation.**<sup>42–49</sup> The open Fabry–Pérot IR microcavity used in this work consists of two Au mirrors, prepared on circular CaF<sub>2</sub> windows ( $d = 25.0$  mm, 5.0 mm thickness) by a high vacuum sputtering (Leica EM MED 020). The thickness of the Au film was controlled using a quartz crystal balance as a reference during sputtering. We used a minimum 10 nm Au thick layer to prepare a uniform film and to avoid metal percolation and unwanted surface enhancement effect. The open cavity structure is realized by mounting the Au-coated CaF<sub>2</sub> substrates onto a piezo-actuated kinematic mirror mount (Thorlabs, KC1-PZ/M) and positioned a set distance away from each other using a home-built cavity holder. The optical path length of the cavity ( $L_{op}$ ) and the corresponding cavity modes were adjusted by applying a voltage on a piezoelectric element of the upper mirror holder (Figure 1c). The whole cavity assembly was situated in the sample compartment of a Fourier transform infrared (FTIR) spectrometer (Bruker VERTEX 70) to perform the transmission measurements. Our cavity structure enabled us to decrease the  $L_{op}$  of the cavity down to 4–5  $\mu\text{m}$ , with a free spectral range (FRS) of about 1000  $\text{cm}^{-1}$ . Drops of methyl salicylate in methylcyclohexane with an appropriate concentration were deposited onto the edges of the CaF<sub>2</sub> windows with the use of a micropipet until the entire microcavity was filled through capillary action.

**Optical Measurements.** All transmission spectra were recorded with the FTIR spectrometer (Bruker VERTEX 70).

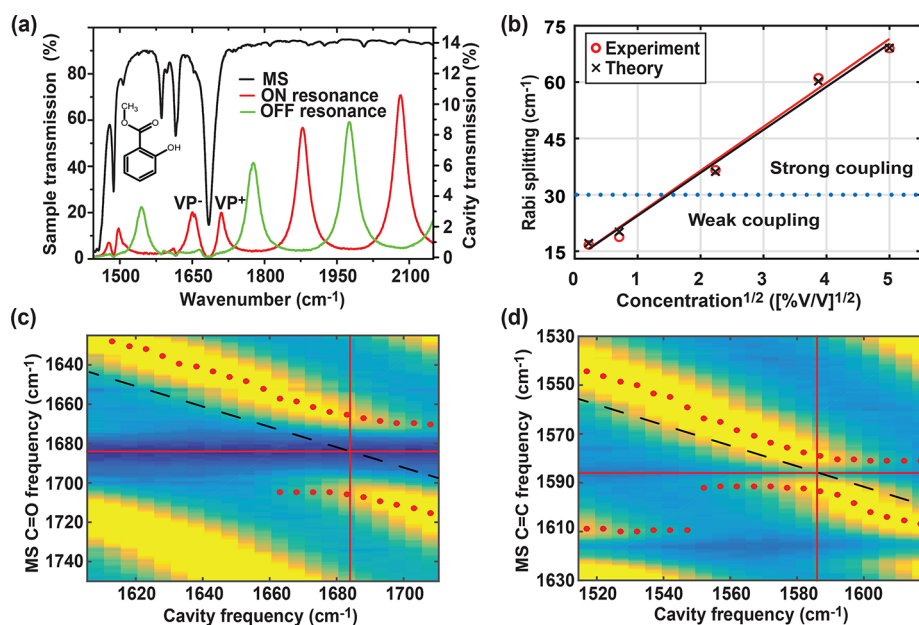


**Figure 2.** (a) FTIR transmission spectrum of 15% v/v MS dissolved in methylcyclohexane (black curve). Transmission spectrum of a microcavity filled with MS solution: on (red) and off (green) resonance, respectively. (b) Concentration dependence of the Rabi splitting of the C=O stretching mode of MS. Experimental and calculated data are shown in red circles and black crosses, respectively, and are obtained from the spectral separation of the  $VP^-$  and  $VP^+$ . The solid red and black lines are linear fits to the experimental and theoretical data, respectively. The dotted line indicates the transition between the weak and strong coupling regimes. The calculated results are taking into account simultaneous coupling of three vibrations to the same cavity mode. (c, d) Dispersion plots for C=O (c) and C=C (d) vibrations of MS (5% v/v) coupled to a microcavity. Dots indicate maxima of the intensity of polaritonic peaks. Solid red lines indicate resonant frequencies of the cavity and C=O and C=C stretching modes, while black dashed lines indicate the cavity mode tuning, highlighting the anticrossing character of the dispersion plot.

Spectra were measured with a resolution of  $0.5\text{ cm}^{-1}$  and averaged over 50 subsequent scans. MS solutions (0.05, 0.5, 5, 15, and 25% v/v) were prepared by dissolving MS in methylcyclohexane. The free space transmission spectra of neat MS and neat BN were obtained by injecting the liquid between two uncoated  $\text{CaF}_2$  windows. Prior to vibrational strong coupling experiments, the quality of an empty cavity was verified by measuring its transmission spectrum. Then the cavity was filled with a solution and a voltage applied to the piezo element was adjusted in order to tune the cavity mode toward the molecular mode under study.

**Theoretical Description by Coupled Oscillators.** In order to theoretically describe VSC, we used up to four coupled damped harmonic oscillators; one oscillator is used to model the cavity mode and the other three oscillators are used to model the three different molecular vibrations coupling to the same cavity mode. The four equations of motion of such a coupled oscillator system can be written as follows:<sup>50,51</sup>

$$\ddot{x}_1(t) + \gamma_1 \dot{x}_1(t) + \omega_1^2 x_1(t) + \kappa_2 x_2(t) + \kappa_3 x_3(t) + \kappa_4 x_4(t) = 0 \quad (1)$$

$$\ddot{x}_2(t) + \gamma_2 \dot{x}_2(t) + \omega_2^2 x_2(t) + \kappa_2 x_1(t) = 0 \quad (2)$$

$$\ddot{x}_3(t) + \gamma_3 \dot{x}_3(t) + \omega_3^2 x_3(t) + \kappa_3 x_1(t) = 0 \quad (3)$$

$$\ddot{x}_4(t) + \gamma_4 \dot{x}_4(t) + \omega_4^2 x_4(t) + \kappa_4 x_1(t) = 0 \quad (4)$$

with the damping constants  $\gamma_1$ ,  $\gamma_2$ ,  $\gamma_3$ , and  $\gamma_4$ , resonance frequencies  $\omega_1$ ,  $\omega_2$ ,  $\omega_3$ , and  $\omega_4$ , and coupling constants  $\kappa_2$ ,  $\kappa_3$ , and  $\kappa_4$ . Equation 1 is used to describe the cavity mode and is coupled to eqs 2–4 via the terms proportional to  $\kappa$ , which allows a coherent energy exchange between the cavity mode

$x_1(t)$  and the vibrations  $x_{2-4}(t)$ . We solved these coupled differential equations numerically to obtain the time evolution of the amplitudes  $x_{1-4}(t)$ , and their Fourier transforms yielded the corresponding spectrum. Especially interesting is the time evolution of the cavity mode  $x_1(t)$ , since it corresponds to the transmission spectrum of the coupled system and can be measured experimentally. This calculated transmission spectrum can be fitted to the experimental data and different scenarios can be evaluated, which are shown in Figure 4. The parameters used to simulate the spectra shown in Figures 3 and 4 are given in Table S2 for benzonitrile and in Tables S3 and S4 for MS.

## RESULTS AND DISCUSSION

The design of the piezo-based tunable Fabry–Pérot open microcavity is presented in Figure 1c.<sup>42–49</sup> In a nutshell, the cavity consists of two Au-coated  $\text{CaF}_2$  windows (see Methods). The two mirrors are mounted into mirror holders, and the optical path length ( $L_{\text{op}}$ ) of the cavity is tuned by applying a voltage to the piezoelectric stacks integrated in one of the mirror mounts. The exemplary transmission spectra of an empty microcavity as a function of applied voltage are shown in Figure 1d. For each voltage increment (1 V),  $5\text{ cm}^{-1}$  shift of the resonant frequency is observed. A typical Q-factor of 70–100 was achieved and the optical path length was varied ( $L_{\text{op}} \sim 12\text{--}30\ \mu\text{m}$ ) depending on the concentration of the sample, yielding the free spectral range (FSR) in the range 200–400  $\text{cm}^{-1}$ . The microcavity employed in this work has the advantage that the parallelism of the cavity mirrors can still be controlled after assembly, along with a nearly unlimited tuning range, and can be used for coupling of the cavity mode with essentially any molecular vibration in the mid-infrared region, at normal incidence. This makes our cavity setting a

versatile device for VSC controlled chemical kinetics studies.<sup>34,35</sup>

The FTIR spectrum of MS diluted in methylcyclohexane is shown in black in Figure 2a. It exhibits an intense C=O stretching frequency at 1685 cm<sup>-1</sup>. The vibrational frequency of free aromatic C=O ester residues usually between 1735 and 1750 cm<sup>-1</sup>.<sup>52</sup> In MS hydrogen bonding leads to a red shift of the C=O stretching frequency, which is consistent with values reported in the literature.<sup>53,54</sup> The bands observed at 1585 and 1616 cm<sup>-1</sup> in the FTIR spectrum of MS arise from C=C vibrational stretching modes of the phenyl moiety.<sup>55</sup>

In order to create the vibrational polaritonic states in MS, the cavity was tuned toward the C=O vibrational band. On resonance, two new transitions, at 1650 and 1710 cm<sup>-1</sup>, are observed in the transmission spectrum of the coupled system (Figure 2a, red curve). These are the signatures of the vibrational hybrid light–matter states (VP<sup>-</sup> and VP<sup>+</sup>) in MS. In the off-resonance case (Figure 2a, green curve) the VSC effect is not observed, yet a minute dispersive line shape is detected at the vibrational mode frequency. The separation between VP<sup>+</sup> and VP<sup>-</sup> (60 cm<sup>-1</sup>)—the Rabi splitting—is larger than the line width of the cavity mode (30 cm<sup>-1</sup>) and of the molecular resonance (16 cm<sup>-1</sup>). Since the coupling exceeds the line widths of both resonator and molecule, the hybridization of the cavity mode and the C=O transition in MS satisfies the criterion of the strong coupling.<sup>14</sup>

Changing the concentration of MS in the mode volume of the cavity leads to an increase of the observed Rabi splitting,<sup>6,26</sup> which is shown experimentally in red circles in Figure 2b. The solid lines are linear fits to the data. At the lowest concentrations (0.05 and 0.5% v/v), the values of the Rabi splitting are smaller than the bandwidth of the cavity mode. However, when the concentration increases to 5% v/v, the value of the splitting energy exceeds the bandwidth of the cavity and the coupled system passes from the weak to the strong coupling regime. The black crosses display the peak separation calculated with a harmonic oscillator approach, which is discussed below and in Methods. Figure 2c,d displays the polariton anticrossing behavior as a function of the cavity tuning. The bare C=O vibration and the bare cavity mode cross each other (marked by two red lines in Figure 2c), while the maxima of the VP<sup>+</sup> and VP<sup>-</sup> show avoided crossing, which is yet another signature of the strong coupling in MS.

The theoretical description of VSC is based on coupling of up to four damped harmonic oscillators and is described in Methods and by Junginger et al.<sup>50</sup> The equations of motion for the amplitudes of the coupled harmonic oscillators are described by differential equations, as shown in Methods. The time evolution of the amplitudes is obtained by solving these equations numerically. The transmission spectra were obtained by Fourier transformation of the amplitudes. The molecular and cavity damping constants were obtained from the full width at half-maxima of the free space transmission spectra of MS and the off-resonant cavity mode, respectively. These parameters were kept constant during all simulations. The parameters which are varied and used to fit the experimental spectrum are the coupling constants and the spectral position of the cavity mode. Benzonitrile (BN) was used as a simple model compound, since it has a well-isolated C≡N vibration. Figure 3a,b shows the experimental (blue line) and simulated (red line) transmission spectra of a cavity containing neat benzonitrile. The dashed vertical lines indicate

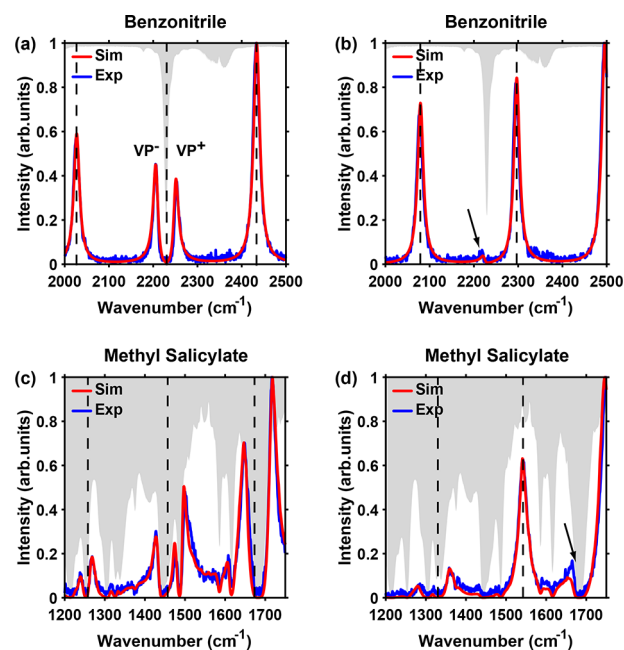


**Figure 3.** (a, b) Experimental (blue line) and simulated (red line) cavity transmission spectra. The cavity is on resonance in (a) and off resonance in (b) with the C≡N vibration of benzonitrile. A splitting into the lower (VP<sup>-</sup>) and upper (VP<sup>+</sup>) vibrational polaritons is clearly observable. The free space transmission spectrum is indicated by the gray area. (c, d) Experimental (blue) and simulated (red line) transmission spectra of methyl salicylate in an on-resonance (c) and off-resonance cavity (d). The transmission spectrum exhibits a complex mode coupling. The transmission spectrum of MS solution (25% v/v) is indicated by the gray area. The dashed lines indicate the cavity modes.

the three cavity resonances. The gray area illustrates the free space transmission spectrum of a BN solution.

In Figure 3a splitting into the lower (VP<sup>-</sup>) and upper (VP<sup>+</sup>) vibrational polaritons can be observed in the transmission spectrum when the C≡N stretching mode at 2229 cm<sup>-1</sup> is hybridized with the cavity mode. The separation between the VP<sup>+</sup> and VP<sup>-</sup> peaks is 50 cm<sup>-1</sup>, which is comparable with values reported by George et al.<sup>26</sup> The experimental (blue line) and simulated (red line) transmission spectra of the same cavity are shown in Figure 3b, but in this case the cavity resonance is detuned from the C≡N vibration. The transmission spectrum is similar to an empty cavity, and only a weak signature of coupling is observed (marked with an arrow). We found a very good agreement between the experimental and simulated data, which shows that the coupled oscillator approach is suitable to model the strongly coupled molecule–cavity hybrid system. Panels c and d of Figure 3 show an equivalent experiment with MS in on- and off-resonant cavities, respectively. When one of the cavity resonances is tuned toward the C=O vibrational band at 1685 cm<sup>-1</sup>, the Rabi splitting is observed in the transmission spectrum of the coupled system (Figure 3c). Two other cavity resonances are located at 1275 and 1465 cm<sup>-1</sup>, and the mode splitting is more complex due to coupling of multiple vibrations to the same cavity mode. Figure 3d shows the cavity transmission spectrum for another cavity length, where one cavity mode at 1323 cm<sup>-1</sup> couples to vibrations in this spectral range, while two cavity modes at 1533 and 1730 cm<sup>-1</sup> are off resonant to the strongest vibrations. Nevertheless,

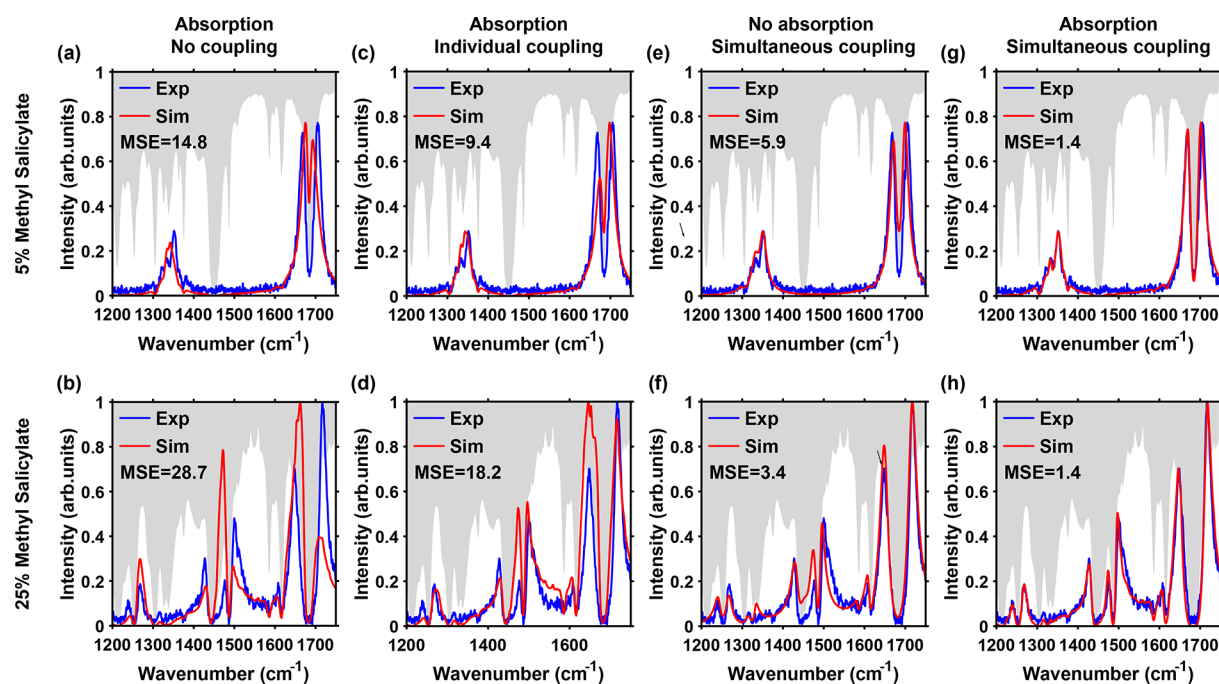


**Figure 4.** (a, b) Experimental (blue line) cavity transmission for 5 (a) and 25% v/v (b) solutions of MS inside an on-resonant cavity. The respective transmission spectrum of MS in free space is always indicated by the gray area. MSE indicates the mean square error and is a measure of the fit quality. The calculated spectrum shown in red only includes the absorption of MS and no VSC is considered. In (c) and (d) the same experimental (blue lines) transmission spectra are shown, but they are compared to simulations (red lines) taking into account the absorption of the sample and strong coupling of the vibrations that are resonant with the respective cavity mode. (e, f) The case when, in addition to resonant coupling of the cavity with a molecular mode, simultaneously also the closest two off-resonant molecular vibrations are allowed to couple to the cavity mode. Finally, the simulations in (g) and (h) include absorption and simultaneous coupling of vibrations, which are spectrally close to the cavity mode.

coupling to the intense C=O stretching vibration can still be observed at  $1685\text{ cm}^{-1}$  (indicated by the arrow in Figure 3d), even though the cavity is not resonant to this vibration. Such an off-resonant coupling is observed for various vibrations, e.g., at  $1458$  and  $1616\text{ cm}^{-1}$ , and is characterized by weak dispersive line shapes in the cavity transmission spectrum.

The transmission spectrum of a cavity containing MS is obviously more complex than that for BN, since MS has a richer vibrational spectrum and multiple vibrations are spectrally close enough to couple to the same cavity mode. In the following, we investigate this coupling behavior in detail. Figure 4 shows the experimental (blue lines) transmission spectra of 5% v/v (top row) and 25% v/v (bottom row) solutions in a resonant cavity together with the corresponding simulations (red lines). The transmission spectrum of a bare MS solution with the same concentration is given by the gray area.

Figure 4 compares four simulated coupling scenarios with the experimental transmission spectra of an on-resonance cavity. In the first case (Figure 4a,b) coupling of MS to the cavity mode is switched off in the simulations and only absorption of uncoupled MS molecules is considered. Absorption needs to be taken into account, since the number of coupled molecules in the cavity volume is much smaller than the number of uncoupled molecules.<sup>41</sup> This is achieved by calculating the cavity transmission spectrum and multiplying it with the free space MS transmission spectrum. This operation leads to a splitting of the originally Lorentzian shaped cavity transmission spectrum, even though there is no VSC. However, there are various discrepancies between the calculated spectrum and the experimental spectrum, especially

the dip at  $1685\text{ cm}^{-1}$ , and the intensity ratios of all peaks are not reproduced well, leading to large mean square errors (MSEs) of 14.8 and 28.7, respectively. Evidently, considering only absorption of uncoupled molecules is not sufficient to model the experimental transmission spectrum. In the second case (Figure 4c,d) we take both absorption and VSC into account, but different MS vibrations couple individually to the cavity modes. Similar to Figure 4a,b, we find a splitting of the cavity transmission spectrum into several modes, but the intensity ratios of the modes at  $1465$  and  $1685\text{ cm}^{-1}$  are not fitting the experimental data. Nevertheless, the MSEs reduce to 9.4 and 18.2. The last two cases illustrate the effect when in addition to resonant coupling of the cavity with a molecular mode simultaneously also the closest two off-resonant molecular vibrations are allowed to couple to the respective cavity mode without (Figure 4e,f) and with (Figure 4g,h) inclusion of absorption of uncoupled molecules. The agreement between the experimental data and the simulation increases when simultaneous coupling of the cavity mode with vibrations, which are spectrally close (see Figures S2 and S3 for assignment of the vibrations), is considered and the MSEs decrease to 5.9 and 3.4, respectively. However, we find the best match between the simulation and the experimental data when simultaneous coupling and absorption are taken into account (Figure 4g,h) with a MSE of 1.4 for both concentrations. It is evident that absorption of uncoupled molecules needs to be considered and that we observe simultaneous hybridization of, at least, three MS vibrations with the same cavity mode. This simultaneous coupling mainly influences the intensity of the modes, while the Rabi splitting is less affected. This is in agreement with the change of the Hopfield coefficients

reported in refs 29 and 40. Additionally, we compare this coupled oscillator approach with the transfer matrix method, which is shown in Figure S5. The transfer matrix method is able to reproduce the main features of the experimental data, but we find smaller MSEs for the coupled oscillator approach, which additionally allows us to determine coupling and damping constants. We compared the widths of polaritons from the theoretical and experimental spectra, and the match is much better for the coupled oscillators model. The polariton peaks calculated from the coupled oscillator model differ at most by 9/8% from the experimental data for 5/25% MS solution, while for the transfer matrix method model the discrepancy reaches 27/30%, respectively. Moreover, the observed polariton bands are narrower than expected based on the average value of the bandwidths of the cavity mode and vibrational band. While vibrational modes are inhomogeneously broadened, it is the homogeneous component, which is narrower, that contributes to the coupling and formation of polariton peaks.<sup>56</sup> Hence, the measured polariton peaks are narrower than the calculated ones, where inhomogeneous bandwidth was taken into account. Finally, we can compare the experimental Rabi splitting with the corresponding calculations, which are shown in Figure 2b. The Rabi splitting of the experimental spectrum, obtained from the spectral separation between  $VP^-$  and  $VP^+$  peaks, is shown in red in Figure 2b. The black crosses in Figure 2b show the peak separation in the calculated spectra, and there is an excellent agreement with the experimental values.

## CONCLUSIONS

In summary, the open Fabry–Pérot microcavity used in this work is an appropriate tool for the emerging fields where vibrational strong coupling plays a central role, as it can be fine-tuned to any molecular vibration. We found that, in addition to resonant coupling of a molecular vibration to a cavity mode, also coupling of the closest off-resonance molecular vibrations has to be taken into account for a good reproduction of the experimental spectra. This is an important observation, as it suggests that coupling, and therefore energy transfer, occurs even for molecular modes that are off-resonant but close to a cavity resonance. We showed that the complex coupling pattern between multiple molecular transitions with a single cavity mode is well captured by the coupled harmonic oscillator model. The best correspondence between the theory and experiment is found when the effects of absorption of uncoupled molecules and simultaneous coupling of close off-resonant modes are taken into account.

## ASSOCIATED CONTENT

### Supporting Information

The Supporting Information is available free of charge at <https://pubs.acs.org/doi/10.1021/acs.jpbc.0c03815>.

Methyl salicylate vibrational frequency peak assignments, parameters used to simulate the spectra of benzonitrile and methyl salicylate, comparison of FTIR transmission spectra of methyl salicylate and pure methylcyclohexane, effect of cavity tuning on C=C phenyl stretching and C=O stretching, and theoretical description by transfer matrix (PDF)

## AUTHOR INFORMATION

### Corresponding Authors

**Frank Wackenhut** – Institute of Physical and Theoretical Chemistry and LISA+, University of Tübingen, D-72076 Tübingen, Germany; [orcid.org/0000-0001-6554-6600](https://orcid.org/0000-0001-6554-6600); Email: [frank.wackenhut@uni-tuebingen.de](mailto:frank.wackenhut@uni-tuebingen.de)

**Lukasz Piatkowski** – Institute of Physical Chemistry, Polish Academy of Sciences, 01-224 Warsaw, Poland; Faculty of Materials Engineering and Technical Physics, Poznan University of Technology, 60-965 Poznan, Poland; [orcid.org/0000-0002-1226-2257](https://orcid.org/0000-0002-1226-2257); Email: [lukasz.j.piatkowski@put.poznan.pl](mailto:lukasz.j.piatkowski@put.poznan.pl)

### Authors

**Wassie Mersha Takele** – Institute of Physical Chemistry, Polish Academy of Sciences, 01-224 Warsaw, Poland; Institute of Physical and Theoretical Chemistry and LISA+, University of Tübingen, D-72076 Tübingen, Germany

**Alfred J. Meixner** – Institute of Physical and Theoretical Chemistry and LISA+, University of Tübingen, D-72076 Tübingen, Germany; [orcid.org/0000-0002-0187-2906](https://orcid.org/0000-0002-0187-2906)

**Jacek Waluk** – Institute of Physical Chemistry, Polish Academy of Sciences, 01-224 Warsaw, Poland; Faculty of Mathematics and Science, Cardinal Stefan Wyszyński University, 01-815 Warsaw, Poland; [orcid.org/0000-0001-5745-583X](https://orcid.org/0000-0001-5745-583X)

Complete contact information is available at: <https://pubs.acs.org/10.1021/acs.jpbc.0c03815>

### Author Contributions

<sup>†</sup>F.W. and L.P.: These authors contributed equally.

### Notes

The authors declare no competing financial interest.

## ACKNOWLEDGMENTS

W.M.T. acknowledges support from the European Union's Horizon 2020 research and innovation program under Marie Skłodowska-Curie Grant Agreement No. 711859 (CO-FUND NaMeS project) and financial resources from the Ministry of Science of Poland for science in the years 2017–2021 awarded for the implementation of an international cofinanced project. The project has received funding from the National Science Centre, Poland, Grants 2015/19/P/ST4/03635 and 2017/26/M/ST4/00872, POLONEZ 1, and 2016/22/A/ST4/00029, and from the European Union's Horizon 2020 research and innovation program under Marie Skłodowska-Curie Grant Agreement No. 665778. F.W. and A.J.M. acknowledge support from DFG Grant ME 1600/13-3. The authors thank the reviewer for constructive criticism that helped to improve the quality of the manuscript.

## REFERENCES

- (1) Hertzog, M.; Wang, M.; Mony, J.; Börjesson, K. Strong Light-Matter Interactions: A New Direction within Chemistry. *Chem. Soc. Rev.* **2019**, *48*, 937–961.
- (2) Wang, H.; Wang, H.; Sun, H.; Cerea, A.; Toma, A.; Angelis, F. D.; Jin, X.; Razzari, L.; Cojoc, D.; Catone, D.; Huang, F.; Proietti Zaccaria, R. Dynamics of Strongly Coupled Hybrid States by Transient Absorption Spectroscopy. *Adv. Funct. Mater.* **2018**, *28*, 1801761.
- (3) Hugall, J. T.; Singh, A.; van Hulst, N. F. Plasmonic Cavity Coupling. *ACS Photonics* **2018**, *5*, 43–53.
- (4) Byrnes, T.; Kim, N. Y.; Yamamoto, Y. Exciton-Polariton Condensates. *Nat. Phys.* **2014**, *10*, 803–813.

- (5) Lange, C.; Cancellieri, E.; Panna, D.; Whittaker, D. M.; Steger, M.; Snoke, D. W.; Pfeiffer, L. N.; West, K. W.; Hayat, A. Ultrafast Control of Strong Light–Matter Coupling. *New J. Phys.* **2018**, *20*, 013032.
- (6) Dovzhenko, D. S.; Ryabchuk, S. V.; Rakovich, Y. P.; Nabiev, I. R. Light–Matter Interaction in the Strong Coupling Regime: Configurations, Conditions, and Applications. *Nanoscale* **2018**, *10*, 3589–3605.
- (7) Barnes, W. L. Ensemble Strong Coupling. *New J. Phys.* **2015**, *17*, 081001.
- (8) Flick, J.; Rivera, N.; Narang, P. Strong Light–Matter Coupling in Quantum Chemistry and Quantum Photonics. *Nanophotonics* **2018**, *7*, 1479–1501.
- (9) Baranov, D. G.; Wersäll, M.; Cuadra, J.; Antosiewicz, T. J.; Shegai, T. Novel Nanostructures and Materials for Strong Light–Matter Interactions. *ACS Photonics* **2018**, *5*, 24–42.
- (10) Cao, E.; Lin, W.; Sun, M.; Liang, W.; Song, Y. Exciton–Plasmon Coupling Interactions: From Principle to Applications. *Nanophotonics* **2018**, *7*, 145–167.
- (11) Kolaric, B.; Maes, B.; Clays, K.; Durt, T.; Caudano, Y. Strong Light–Matter Coupling as a New Tool for Molecular and Material Engineering: Quantum Approach. *Adv. Quantum Technol.* **2018**, *1*, 1800001.
- (12) Vasa, P.; Lienau, C. Strong Light–Matter Interaction in Quantum Emitter/Metal Hybrid Nanostructures. *ACS Photonics* **2018**, *5*, 2–23.
- (13) Ebbesen, T. W. Hybrid Light–Matter States in a Molecular and Material Science Perspective. *Acc. Chem. Res.* **2016**, *49*, 2403–2412.
- (14) Törmä, P.; Barnes, W. L. Strong Coupling between Surface Plasmon Polaritons and Emitters: A Review. *Rep. Prog. Phys.* **2015**, *78*, 013901.
- (15) Su, R.; Diederichs, C.; Wang, J.; Liew, T. C.; Zhao, J.; Liu, S.; Xu, W.; Chen, Z.; Xiong, Q. Room-Temperature Polariton Lasing in All-Inorganic Perovskite Nanoplatelets. *Nano Lett.* **2017**, *17*, 3982–3988.
- (16) Zhong, X.; Chervy, T.; Wang, S.; George, J.; Thomas, A.; Hutchison, J. A.; Devaux, E.; Genet, C.; Ebbesen, T. W. Non-Radiative Energy Transfer Mediated by Hybrid Light–Matter States. *Angew. Chem., Int. Ed.* **2016**, *55*, 6202–6206.
- (17) Orgiu, E.; George, J.; Hutchison, J. A.; Devaux, E.; Dayen, J. F.; Doudin, B.; Stellacci, F.; Genet, C.; Schachenmayer, J.; Genes, C.; Pupillo, G.; Samori, P.; Ebbesen, T. W. Conductivity in Organic Semiconductors Hybridized with the Vacuum Field. *Nat. Mater.* **2015**, *14*, 1123–1129.
- (18) Tanyi, E. K.; Thuman, H.; Brown, N.; Koutsares, S.; Podolskiy, V. A.; Noginov, M. A. Control of the Stokes Shift with Strong Coupling. *Adv. Opt. Mater.* **2017**, *5*, 1600941.
- (19) Wang, S.; Chervy, T.; George, J.; Hutchison, J. A.; Genet, C.; Ebbesen, T. W. Quantum Yield of Polariton Emission from Hybrid Light–Matter States. *J. Phys. Chem. Lett.* **2014**, *5*, 1433–1439.
- (20) Hutchison, J. A.; Liscio, A.; Schwartz, T.; Canaguier-Durand, A.; Genet, C.; Palermo, V.; Samori, P.; Ebbesen, T. W. Tuning the Work-Function Via Strong Coupling. *Adv. Mater.* **2013**, *25*, 2481–2485.
- (21) Yuen-Zhou, J.; Menon, V. M. Polariton Chemistry: Thinking inside the (Photon) Box. *Proc. Natl. Acad. Sci. U. S. A.* **2019**, *116*, 5214–5216.
- (22) Kéna-Cohen, S.; Yuen-Zhou, J. Polariton Chemistry: Action in the Dark. *ACS Cent. Sci.* **2019**, *5*, 386–388.
- (23) Campos-Gonzalez-Angulo, J.; Ribeiro, R. F.; Yuen-Zhou, J. Resonant Catalysis of Thermally Activated Chemical Reactions with Vibrational Polaritons. *Nat. Commun.* **2019**, *10*, 4685.
- (24) Ribeiro, R. F.; Martínez-Martínez, L. A.; Du, M.; Campos-Gonzalez-Angulo, J.; Yuen-Zhou, J. Polariton Chemistry: Controlling Molecular Dynamics with Optical Cavities. *Chem. Sci.* **2018**, *9*, 6325–6339.
- (25) Hertzog, M.; Rudquist, P.; Hutchison, J. A.; George, J.; Ebbesen, T. W.; Börjesson, K. Voltage-Controlled Switching of Strong Light – Matter Interactions Using Liquid Crystals. *Chem. - Eur. J.* **2017**, *23*, 18166–18170.
- (26) George, J.; Shalabney, A.; Hutchison, J. A.; Genet, C.; Ebbesen, T. W. Liquid-Phase Vibrational Strong Coupling. *J. Phys. Chem. Lett.* **2015**, *6*, 1027–1031.
- (27) Shalabney, A.; George, J.; Hutchison, J.; Pupillo, G.; Genet, C.; Ebbesen, T. W. Coherent Coupling of Molecular Resonators with a Microcavity Mode. *Nat. Commun.* **2015**, *6*, 5981.
- (28) Ahn, W.; Vurgaftman, I.; Dunkelberger, A. D.; Owrutsky, C.; Simpkins, B. S. Vibrational Strong Coupling Controlled by Spatial Distribution of Molecules within the Optical Cavity. *ACS Photonics* **2018**, *5*, 158–166.
- (29) Muallem, M.; Palatnik, A.; Nessim, G. D.; Tischler, Y. R. Strong Light–Matter Coupling and Hybridization of Molecular Vibrations in a Low-Loss Infrared Microcavity. *J. Phys. Chem. Lett.* **2016**, *7*, 2002–2008.
- (30) Casey, S. R.; Sparks, J. R. Vibrational Strong Coupling of Organometallic Complexes. *J. Phys. Chem. C* **2016**, *120*, 28138–28143.
- (31) Crum, V. F.; Casey, S. R.; Sparks, J. R. Photon-Mediated Hybridization of Molecular Vibrational States. *Phys. Chem. Chem. Phys.* **2018**, *20*, 850–857.
- (32) Thomas, A.; George, J.; Shalabney, A.; Dryzhakov, M.; Varma, S. J.; Moran, J.; Chervy, T.; Zhong, X.; Devaux, E.; Genet, C.; Hutchison, J. A.; Ebbesen, T. W. Ground-State Chemical Reactivity under Vibrational Coupling to the Vacuum Electromagnetic Field. *Angew. Chem., Int. Ed.* **2016**, *55*, 11462–11466.
- (33) Lather, J.; Bhatt, P.; Thomas, A.; Ebbesen, T. W.; George, J. Cavity Catalysis by Cooperative Vibrational Strong Coupling of Reactant and Solvent Molecules. *Angew. Chem., Int. Ed.* **2019**, *58*, 10635–10638.
- (34) Thomas, A.; Lethuillier-Karl, L.; Nagarajan, K.; Vergauwe, R. M. A.; George, J.; Chervy, T.; Shalabney, A.; Devaux, E.; Genet, C.; Moran, J.; Ebbesen, T. W. Tilting a Ground-State Reactivity Landscape by Vibrational Strong Coupling. *Science* **2019**, *363*, 615–619.
- (35) Vergauwe, R. M. A.; Thomas, A.; Nagarajan, K.; Shalabney, A.; George, J.; Chervy, T.; Seidel, M.; Devaux, E.; Torbeev, V.; Ebbesen, T. W. Modification of Enzyme Activity by Vibrational Strong Coupling of Water. *Angew. Chem., Int. Ed.* **2019**, *58*, 15324–15328.
- (36) Frontiera, R. R.; Fang, C.; Dasgupta, J.; Mathies, R. A. Probing Structural Evolution Along Multidimensional Reaction Coordinates with Femtosecond Stimulated Raman Spectroscopy. *Phys. Chem. Chem. Phys.* **2012**, *14*, 405–414.
- (37) Kijak, M.; Nosenko, Y.; Singh, A.; Thummel, R. P.; Waluk, J. Mode-Selective Excited-State Proton Transfer in 2-(2'-Pyridyl)-Pyrrole Isolated in a Supersonic Jet. *J. Am. Chem. Soc.* **2007**, *129*, 2738–2739.
- (38) Waluk, J. Spectroscopy and Tautomerization Studies of Porphycenes. *Chem. Rev.* **2017**, *117*, 2447–2480.
- (39) Menghrajani, K. S.; Fernandez, H. A.; Nash, G. R.; Barnes, W. L. Hybridization of Multiple Vibrational Modes via Strong Coupling Using Confined Light Fields. *Adv. Opt. Mater.* **2019**, *7*, 1900403.
- (40) Imran, I.; Nicolai, G. E.; Stavinski, N. D.; Sparks, J. R. Tuning Vibrational Strong Coupling with Co-Resonators. *ACS Photonics* **2019**, *6*, 2405–2412.
- (41) Erwin, J. D.; Smotzer, M.; Coe, J. V. Effect of Strongly Coupled Vibration-Cavity Polaritons on the Bulk Vibrational States within a Wavelength-Scale Cavity. *J. Phys. Chem. B* **2019**, *123*, 1302–1306.
- (42) Chizhik, A.; Schleifenbaum, F.; Gutbrod, R.; Chizhik, A.; Khoptyar, D.; Meixner, A. J.; Enderlein, J. Tuning the Fluorescence Emission Spectra of a Single Molecule with a Variable Optical Subwavelength Metal Microcavity. *Phys. Rev. Lett.* **2009**, *102*, 073002.
- (43) Mochalov, K. E.; Vaskan, I. S.; Dovzhenko, D. S.; Rakovich, Y. P.; Nabiev, I. A Versatile Tunable Microcavity for Investigation of Light–Matter Interaction. *Rev. Sci. Instrum.* **2018**, *89*, 053105.
- (44) Bär, S.; Chizhik, A.; Gutbrod, R.; Schleifenbaum, F.; Chizhik, A.; Meixner, A. J. Microcavities: Tailoring the Optical Properties of Single Quantum Emitters. *Anal. Bioanal. Chem.* **2010**, *396*, 3–14.

(45) Dolan, P. R.; Adekanye, S.; Trichet, A. A. P.; Johnson, S.; Flatten, L. C.; Chen, Y. C.; Weng, L.; Hunger, D.; Chang, H. C.; Castelletto, S.; Smith, J. M. Robust, Tunable, and High Purity Triggered Single Photon Source at Room Temperature Using a Nitrogen-Vacancy Defect in Diamond in an Open Microcavity. *Opt. Express* **2018**, *26*, 7056–7065.

(46) Kern, A. M.; Zhang, D.; Brecht, M.; Chizhik, A. I.; Failla, A. V.; Wackenhut, F.; Meixner, A. J. Enhanced Single-Molecule Spectroscopy in Highly Confined Optical Fields: From  $\lambda/2$ -Fabry-Pérot Resonators to Plasmonic Nano-Antennas. *Chem. Soc. Rev.* **2014**, *43*, 1263–1286.

(47) Chizhik, A. I.; Chizhik, A. M.; Khoptyar, D.; Bär, S.; Meixner, A. J.; Enderlein, J. Probing the Radiative Transition of Single Molecules with a Tunable Microresonator. *Nano Lett.* **2011**, *11*, 1700–1703.

(48) Herskind, P. F.; Dantan, A.; Marler, J. P.; Albert, M.; Drewsen, M. Realization of Collective Strong Coupling with Ion Coulomb Crystals in an Optical Cavity. *Nat. Phys.* **2009**, *5*, 494–498.

(49) Grant, R. T.; Jayaprakash, R.; Coles, D. M.; Musser, A.; De Liberato, S.; Samuel, I. D. W.; Turnbull, G. A.; Clark, J.; Lidzey, D. G. Strong Coupling in a Microcavity Containing  $\beta$ -Carotene. *Opt. Express* **2018**, *26*, 3320–3327.

(50) Junginger, A.; Wackenhut, F.; Stuhl, A.; Blendinger, F.; Brecht, M.; Meixner, A. J. Tunable Strong Coupling of Two Adjacent Optical  $\lambda/2$  Fabry-Pérot Microresonators. *Opt. Express* **2020**, *28*, 485–493.

(51) Konrad, A.; Kern, A. M.; Brecht, M.; Meixner, A. J. Strong and Coherent Coupling of a Plasmonic Nanoparticle to a Subwavelength Fabry-Pérot Resonator. *Nano Lett.* **2015**, *15*, 4423–4428.

(52) Reichenbacher, M.; Popp, J. *Challenges in Molecular Structure Determination*; Springer-Verlag: Berlin, 2012.

(53) Aparicio, S.; Alcalde, R. On the Structure of Liquid Methyl Salicylate: The Role of Intramolecular Hydrogen Bonding. *Eur. J. Chem.* **2010**, *1*, 162–167.

(54) Joseph, J.; Jemmis, E. D. Red-, Blue-, or No-Shift in Hydrogen Bonds: A Unified Explanation. *J. Am. Chem. Soc.* **2007**, *129*, 4620–4632.

(55) Varghese, H. T.; Panicker, C. Y.; Philip, D.; Mannekutla, J. R.; Inamdar, S. R. IR, Raman and SERS Studies of Methyl Salicylate. *Spectrochim. Acta, Part A* **2007**, *66*, 959–963.

(56) Houdré, R.; Stanley, R. P.; Ilegems, M. Vacuum-Field Rabi Splitting in the Presence of Inhomogeneous Broadening: Resolution of a Homogeneous Linewidth in an Inhomogeneously Broadened System. *Phys. Rev. A: At., Mol., Opt. Phys.* **1996**, *53*, 2711–2715.